JOURNAL OF PROPULSION AND POWER
Vol. 24, No. 4, July–August 2008

Effects of Propellant Gases on Thermal Response of Solid Rocket Nozzle Liners

Ki-Young Hwang* and Yoo-Jin Yim†
Agency for Defense Development, Daejon 305-600, Republic of Korea

DOI: 10.2514/1.34368

The propellant formulations, the gas properties in motor chamber, and the aluminum oxide particle sizes for two kinds of solid propellants with approximately 20% aluminum powder have been investigated. The scanning electron microscope photographs of aluminum oxide particles taken from a nozzle entrance show that the aluminized polycaprolactone polyol propellant with 47% volumetric fraction ammonium perchlorate/hexanitro hexaazaisowurtzitane and the bimodal oxidizers, 200/5 μm, can offer greater possibility for increasing aluminum agglomeration than the aluminized hydroxy-terminated polybutadiene propellant with 64% volumetric fraction ammonium perchlorate and the trimodal oxidizers, 400/200/6 μm. The aluminized polycaprolactone polyol propellant with energetic plasticizers results in locally greater mechanical erosion in four circumferential sections of the nozzle entrance in line with grain slots, due to the impingement of large particles. However, the hydroxy-terminated polybutadiene propellant results in greater thermochemical ablation at the blast tube, the throat insert, and the exit cone of rocket nozzle, due to 2.3 times more water and carbon dioxide oxidizing species in exhaust gases than the polycaprolactone polyol propellant.

Nomenclature

A	=	cross-sectional flow area
c_p	=	specific heat of gases at constant pressure
d_p	=	diameter of aluminum oxide particle
E_0	=	activation energy of a chemical reaction
h	=	convective heat transfer coefficient
K_0	=	preexponential factor of a chemical reaction
k	=	mass fraction of the solid residue of material
M_0	=	molecular weight of gas mixture
M_c	=	molecular weight of carbon
P_w	=	pressure at nozzle wall
R	=	ideal gas constant
T_w	=	temperature at nozzle wall
χ_{CO_2}	=	mole fraction of CO_2
χ_{H_2O}	=	mole fraction of H_2O
ρ_0	=	initial density

Subscripts

t	=	conditions at nozzle throat
w	=	wall conditions

I. Introduction

THE nozzle liner of a solid rocket motor (SRM) is used to limit the temperature of the nozzle structure to acceptable levels, while maintaining the nozzle aerodynamic contour as closely as practical against a high thermal flux and chemically reactive environments. To sustain the high temperature, highly reactive, and often particle-laden surrounding flow generated by the combustion of a solid propellant, the nozzle liners conventionally use some ablative materials such as carbon–carbon, carbon–phenolic, silica–phenolic, and so on. Among these materials, some are thermodegradable and undergo a chemical transformation known as pyrolysis producing decomposition gases and brittle solid residue. Also, those materials, and others that are not thermodegradable, can undergo surface recession due to the thermochemical ablation by heterogeneous chemical reactions with the oxidizing chemical species of the surrounding flow, and/or due to the mechanical erosion by aluminum oxide (Al_2O_3) particle impingements [1–3].

The metallized propellants and submerged nozzles have been adopted in many solid rocket motors to improve performance. The widely used metal fuel is an aluminum powder which consists of small spherical particles and is used in a wide variety of composite propellant formulations, constituting approximately 20% of the propellant by weight [4,5]. During rocket combustion, the Al fuel is oxidized into aluminum oxide. These oxide particles tend to agglomerate and grow larger particles. The oxide is in a liquid form during combustion and solidifies in the nozzle as the gas temperature drops. When in the liquid state, the aluminum oxide forms a molten slag which can deposit on walls inside the motor chamber. Because the slag retained in this manner is a dead weight, the slag accumulation constitutes a degradation of motor performance and is undesirable. Moreover, the particles are responsible for undesirable side effects, such as smoke exhaust trails and nozzle erosion. The particle impingement erosion observed in nozzle liners and chamber insulation materials is affected by the presence of aluminum oxide and unburned aluminum in the exhaust gases. Asymmetric mass flux distributions caused by propellant grain slots often increase the impingement erosion in circumferential areas in line with the grain slots [6].

Recently, numerical approaches have been taken in the field of the three-dimensional nature of the SRM internal flow varying with the propellant grain. For example, the research of Chaouat [7] indicated that vortices shed from slots created asymmetric cross-sectional flow. Three dimensionality of the flow or vortical flow is caused by mixing of the flows from slots with the core flow in the port, and is intensified at the converging part of the submerged nozzle. Because the vortical flow affects the diffusion velocity of the mass and the heat crossing the surface boundary layer on the liner materials, it causes circumferentially asymmetric ablation over the converging part of the nozzle. The effect is rapidly attenuated over the diverging part of the nozzle throat downstream. Morstadt [8] also showed that a pair of counter-rotating vortices in the axial direction shed from each of the forward slots of the space shuttle reusable solid rocket motor is

Presented as Paper 4791 at the 44th AIAA/ASME/SAE/ASEE Joint Propulsion Conference & Exhibit, Connecticut Convention Center, Hartford, CT, 20–23 July 2008; received 5 September 2007; revision received 15 January 2008; accepted for publication 4 February 2008.

*Principal Researcher, Precision Guided Missile Research and Development Institute; kiyhwang@hanafos.com. Member AIAA.

†Principal Researcher, Precision Guided Missile Research and Development Institute; eugeneim@unitel.co.kr.

the strongest source of the vortices in the axial direction in the core flow.

The objective of this study is to investigate the thermal response characteristics of nozzle liners for a solid rocket motor with slotted tube grain containing an aluminized polycaprolactone polyol (PCP) or hydroxy-terminated polybutadiene (HTPB) based propellant. The special emphasis is given both on locally greater mechanical erosion by the particle impingement on the nozzle entrance and on thermochemical ablation at the blast tube, the throat insert, and the exit cone of a rocket nozzle by the oxidizing chemical species in exhaust gases.

II. Propellant Characteristics

Aluminum powder is used as an ingredient in solid propellants to increase the propellant density and exhaust gas temperature, resulting in an increase in impulse density of about 10%. Compared with other metal additives, aluminum has the advantages of relatively low cost and good safety, and is therefore used in a wide range of tactical and large booster motors. Table 1 shows the propellant formulations, the densities, and the burning rates for two kinds of aluminized propellants (hereinafter referred to as "propellant *H*" and "propellant *P*"). The sizes of aluminum powder for the two propellants are the same at 25 μm, and the aluminum powders of propellants *H* and *P* constitute 19 and 20% of the propellant by weight, respectively. However, the compositions of both oxidizer and binder for propellant *H* are different from those of propellant *P*. Propellant *H* contains 64% volumetric fraction oxidizer with a trimodal blend of 400/200/6 μm ammonium perchlorate (AP) and 24% volumetric fraction HTPB binder. However, propellant *P* contains 47% volumetric fraction oxidizer with a bimodal blend of 200 μm AP and 5 μm hexanitro hexaazaisowurtzitane (HNIW) and 40% volumetric fraction PCP binder with energetic plasticizers, such as trimethylol ethane trinitrate (TMETN) and butane triol trinitrate (BTTN) [9]. Figure 1 shows the distributions of oxidizers, aluminum powders, and binders in propellants *H* and *P*.

It is well known that aluminum powder has a tendency to agglomerate on the burning surface of composite propellants. The sequential picture of agglomeration behavior has evolved from a variety of experimental studies [10,11]. It has become evident that agglomeration is a result of a complex sequence of conditions and processes. These include the initial distribution of aluminum in the propellant matrix and its tendency to accumulate on the burning surface. When the powders of the fine fraction of oxidizer are large enough to substantially fill the voids in the packing array of a relatively coarse oxidizer (Fig. 1a), the aluminum powders are thinly dispersed in the propellant matrix and, hence, if they agglomerate on the burning surface, they must do so in a scattered fashion [12]. The emerging aluminum above the burning surface may agglomerate up to and beyond the contents of individual pockets of the coarse oxidizer. It follows that the smaller the pockets in the matrix, the less the size and extent of agglomerates. Cohen [13] developed a pocket model which explains qualitative effects of propellant formulation and pressure on the extent of aluminum agglomeration in AP/HTPB propellants. The model proposed that trimodal distributions of oxidizers appear to offer greater flexibility for minimizing agglomeration than bimodal formulation. Therefore, it is understandable that propellant *P*, with relatively smaller size and less content of oxidizer, may offer much more favorable conditions for larger agglomerates than propellant *H*.

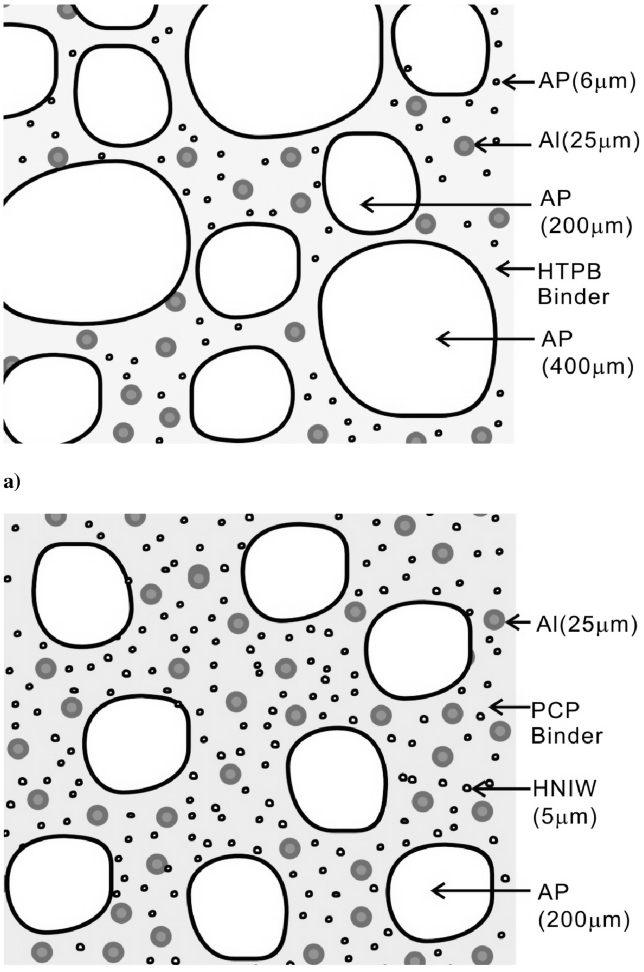

Fig. 1 Schematic diagrams of composition distribution: a) propellant *H* and b) propellant *P*.

The burning of aluminized propellants often produces relatively large Al_2O_3 particles. For aluminized propellants, the alumina particle size depends on many factors, such as propellant formulation, ingredient size, chamber pressure, and aluminum concentration. Particle size distribution of Al_2O_3 in the exhaust gases of rocket motors has been extensively studied since the 1970s, because of its effect on motor performance losses [14], the slag accumulation in the aft end of a submerged nozzle [15,16], and the burning rate of propellants [17,18].

Table 1 Comparison of propellants *H* and *P*

Type	Density, g/cm^3	Burning rate @10.3 MPa, mm/s	Propellant ingredient	Density, g/cm^3	Powder size, μm	Mass fraction, %	Volumetric fraction, %
Propellant *H*	1.80	8.0	HTPB binder	0.91	——	12	24
			AP oxidizer	1.95	400	31	29
			AP oxidizer	1.95	200	31	29
			AP oxidizer	1.95	6	7	6
			Aluminum	2.71	25	19	12
Propellant *P*	1.81	8.3	PCP binder	1.31	——	29	40
			AP oxidizer	1.95	200	31	29
			HNIW oxidizer	2.03	5	20	18
			Aluminum	2.71	25	20	13

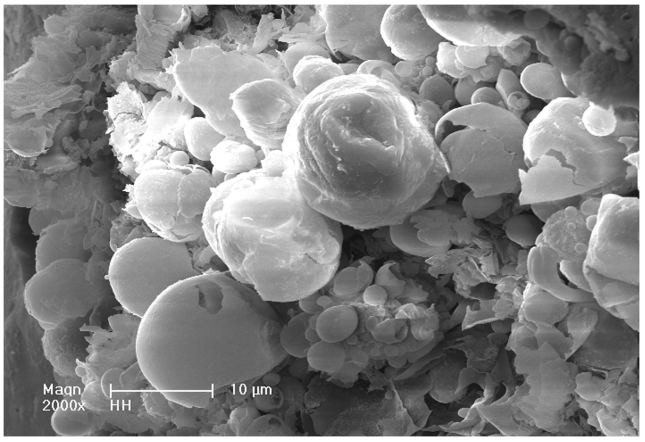

a)

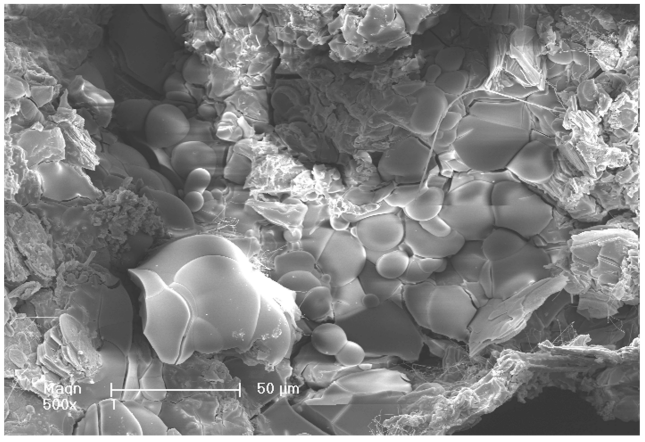

b)

Fig. 2 SEM photographs of aluminum oxide particles: a) propellant *H* and b) propellant *P*.

The PCP binder in propellant *P* contains 17 wt % of energetic plasticizers. Therefore, a large area of the burning surface of propellant *P* is a molten layer. However, propellant *H* keeps a solid burning surface during combustion. According to the combustion mechanisms of composite propellants [19], the molten layer on the burning surface of aluminized composite propellant could provide a positive effect on aluminum agglomeration.

On the base of the preceding description for the aluminum agglomeration in composite propellants, it is worth noting that propellant *P* with 40 vol % active binder (PCP) and bimodal AP/HNIW oxidizers may offer much more favorable conditions for the presence of larger Al_2O_3 particles inside the combustion gases, than propellant *H* with 24 vol % inert binder (HTPB) and trimodal AP oxidizers.

Figure 2 shows the scanning electron microscope (SEM) photographs of the Al_2O_3 particles taken from nozzle entrance liners for two propellants. In the case of propellant *H*, the numerous small round particles were observed with a maximum diameter around 10 μm. On the other hand, in Fig. 2b for propellant *P*, almost all particles were over 10 μm, and larger particles over 50 μm agglomerated from smaller particles could also be seen. From the examination of Al_2O_3 particles by the SEM photographs, it is revealed that the particle sizes for propellant *P* are relatively larger than those for propellant *H*.

Hwang and Chang [20] developed a numerical technique for the calculation of gas–particle flow in a solid rocket nozzle and presented the particle trajectories for four kinds of particle sizes (2, 10, 20, and 40 μm) in an external nozzle. The combustion gas properties and nozzle entrance configuration are similar to those of the present study. As shown in Fig. 3, the number of particles impacting on the convergent part of the nozzle for the small particle (2 μm) is less than that of large particle (40 μm), because the small particles can more easily be parallel to the wall at the convergent part of the nozzle due to their small inertia.

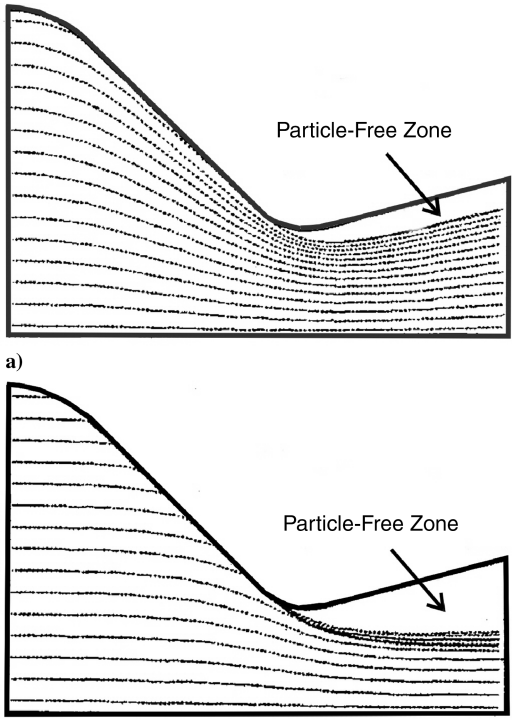

a)

b)

Fig. 3 Trajectories for two sizes of particles in a solid rocket nozzle: a) $d_p = 2$ μm and b) $d_p = 40$ μm [20].

Table 2 shows the combustion gas properties for equilibrium flow in a motor chamber with a pressure of 10.3 MPa for two propellants. Propellant *H* is more than twice as large as propellant *P* in the mole fraction of H_2O and CO_2, but the mass fraction of Al_2O_3 and other thermal properties are similar to those of propellant *P*.

Combustion products from a solid rocket motor are composed of a variety of gases, such as H_2O, CO_2, H_2, CO, and HCl. Gases, such as H_2O, CO_2, O_2, O, OH, and NO, oxidize carbon to CO. However, O_2, O, OH, and NO are present in very low concentrations in typical propellant combustion products. Furthermore, reactions with hydrogen are possible only at very high temperatures of the wall (over 4000 K) [21,22]. Therefore, H_2O and CO_2 are considered to be the major reactive species, and these species react with the carbon of the nozzle surface, as shown by the following reactions:

$$C + CO_2 \rightarrow 2CO \tag{1}$$

$$C + H_2O \rightarrow CO + H_2 \tag{2}$$

Table 2 Gas properties in motor chamber

Parameter	Propellant *H*	Propellant *P*
Gas temperature, K	3576	3588
Molecule weight, kg/kmol	29.754	29.748
Specific heat c_p, J/kg · K	2389	2346
Characteristic velocity, m/s	1574	1575
Viscosity, kg/m · s	95.7E-6	91.9E-6
Prandtl number	0.8724	0.8704
Specific heat ratio	1.1324	1.1352
Mole fraction of H_2O, %	13.05	5.52
Mole fraction of CO_2, %	1.22	0.71
Mass fraction of Al_2O_3, %	30.59	31.64

III. Thermal Response of Rocket Nozzle Liner

A. Nozzle Liner and Ablation Behavior

Figure 4 shows the propellant grain and nozzle geometry of the solid rocket motor used in this study. The motor is about 3 m long, with an outer diameter of 0.275 m. The motor chamber contains propellant *H* or *P* with a neutrally burning grain. The average chamber pressure and burning time are approximately 9 MPa and 10 s, respectively, at an initial propellant temperature of 20°C. Four slots are located at the aft end of the grain, and they merge into a central cylindrical port. The motor has an external nozzle with a blast tube to provide an aft-end packing envelope for movable aerodynamic surfaces and their control systems. The diameter of the nozzle throat is 0.0655 m and the exit cone has a contoured shape with an expansion ratio of 8.6. All of the nozzle liners exposed to the combustion gases are carbonaceous materials, such as carbon/phenolic and graphite, which have shown better resistance to Al_2O_3 particle impingement than silica-based materials forming a molten layer. Polycrystalline graphite (ATJ) is used in the throat insert because of its relatively low cost and good ablation resistance. The manufacturing methods for each liner of the nozzle are also included in Fig. 4.

As the propellant in a rocket motor burns, the nozzle is exposed to hot combustion gases, which form a turbulent boundary layer over the nozzle surface. The hot gases transfer energy to the nozzle, causing its surface temperature to rise rapidly. The high surface temperatures of the nozzle increase the reactivity of the carbonaceous material, and heterogeneous reactions between oxidizing species (H_2O and CO_2) and the carbon begin to occur. Such surface reactions deplete the amount of oxidizing species available at the nozzle surface and thereby create concentration gradients in the flowfield, which cause a diffusion of oxidizing species toward the nozzle surface. Therefore, the rate of nozzle ablation depends on both the chemical kinetic rates of the heterogeneous reactions and the diffusion rate of oxidizing species to the surface. If the kinetic rates are much higher than the diffusion rates, the ablation rate is determined solely by the diffusion rate of oxidizing species. The other extreme case is the high diffusion rates and low kinetic rates, with the ablation rate solely determined by the chemical kinetics. It is well known that the ablation rate of a rocket nozzle is largely determined by the diffusion rate of the oxidizing species to the nozzle surface [23,24]. The influence of chemical kinetics is predominant only during the short initial period of motor firing when the surface temperatures are low.

Considering the processes of heat and mass transfer in a turbulent boundary layer, Boyarintsev and Zvyagin [25] have developed a thermochemical ablation model for a carbonaceous material (graphite). According to the model, the mass recession rate of a carbonaceous material caused by its interaction with the oxidizing species is determined from the following formula:

$$\dot{m} = \left(\frac{h}{c_p}\right)_w B_c \tag{3}$$

In the preceding equation, B_c is the dimensionless mass recession rate, taking into account the two carbon oxidation modes (kinetic and diffusion) as the temperature at the nozzle surface increases, and is calculated from the following formula:

$$B_c = \frac{\sqrt{[(M_c/M_0)\Omega + 1]^2 + 4B_m(M_c/M_0)\Omega} - [(M_c/M_0)\Omega + 1]}{2(M_c/M_0)\Omega} \tag{4}$$

where

$$B_m = \frac{M_c}{M_0}(\chi_{H_2O} + \chi_{CO_2}) \tag{5}$$

$$\Omega = \left(\frac{h}{c_p}\right)_w \left(\frac{T_w}{P_w}\right) \frac{1}{1.465K_0} \exp\left(\frac{E_0}{RT_w}\right) \tag{6}$$

The value of B_c asymptotically reaches the value of the oxidizing potential of the combustion gases B_m as the temperature grows. In the diffusion region, the ablation rate of carbonaceous material is defined by the expression

$$V_s = \left(\frac{h}{c_p}\right)_w \frac{B_m}{k\rho_0} \tag{7}$$

As shown in Table 2, the combustion gas properties of propellant *H* are similar to those of propellant *P*, except for the mole fraction of H_2O and CO_2. When calculating the oxidizing potentials (B_m) for two propellants, it is known that propellant *H* has 2.3 times as much as propellant *P*. Therefore, the thermochemical ablation of the nozzle liner for propellant *H* will be approximately 2.3 times greater than that for propellant *P*, if all characteristics of the motor except the propellant formulation are the same and, also, the ablation rate is largely determined by the diffusion rate of oxidizing species shown in Eqs. (5) and (7).

B. Effects of Two Different Gases on Thermal Response of Nozzle Liner

Figures 5a and 5b show the ablation and char profiles on the two cross sections of the nozzle liner for propellants *H* and *P*,

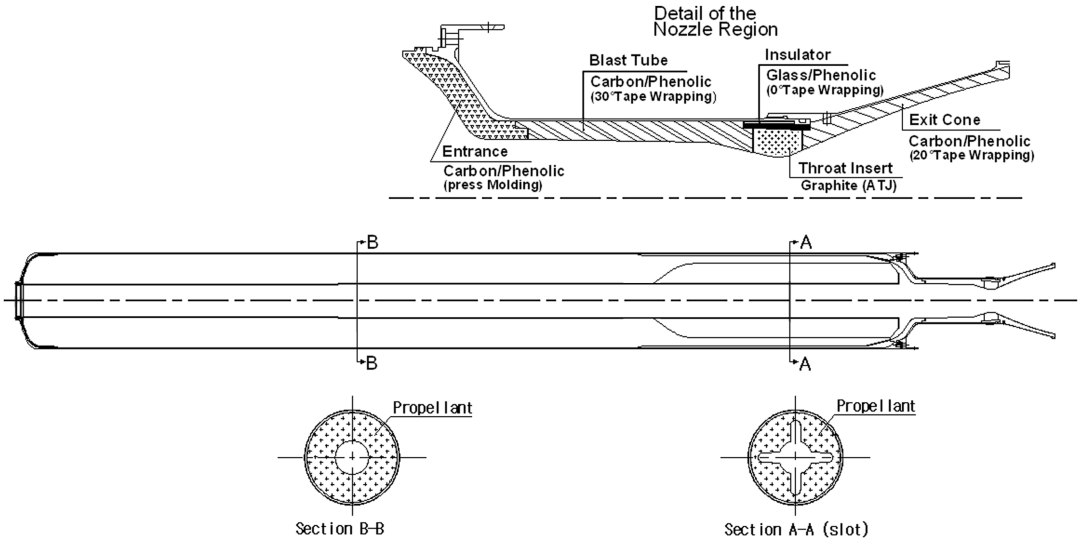

Fig. 4 Propellant grain and nozzle geometry of a solid rocket motor.

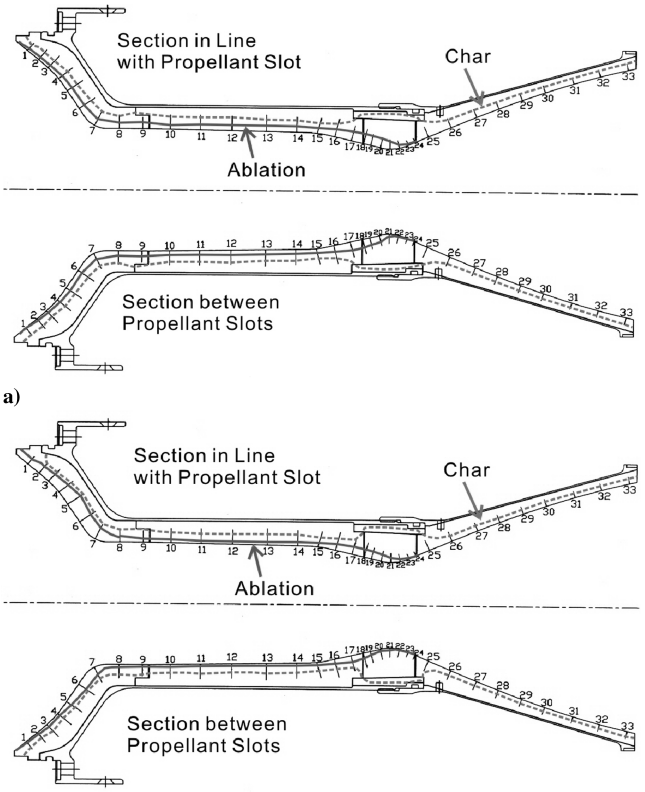

Fig. 5 Ablation and char profiles on two cross sections of nozzle liner: a) propellant *H* and b) propellant *P*.

respectively. The upper part of Figs. 5a and 5b is the section in line with the propellant grain slot, and the lower part is the section between the propellant grain slots. The ablation thicknesses at two sections of the nozzle entrance liner for propellants *H* and *P* are compared in Fig. 6. Included in Fig. 6 are the area ratios for each station number along the entrance liner surface. It can be seen in Figs. 5a and 6 that the ablation thickness and char depth of the entrance liner for propellant *H* are almost identical at two cross sections, but the ablation thicknesses increase with decreasing area ratio because a decrease in the area ratio causes an increase in the convective heat flux at the entrance liner. This indicates that the ablation and char characteristics of the entrance liner for propellant *H* are nearly the same throughout any section of a circumferential angle, regardless of the propellant grain slots. However, the asymmetry in erosion (ablation) at the entrance liner for propellant *P* can be seen in Figs. 5b and 7b. Also, the aluminum oxide particles are deposited on the liner, as shown in Fig. 7b. The four isolated and more severe erosion regions observed when applying propellant *P* were at approximately 90 deg intervals in the circumferential direction, and also appeared at the directions which are coincident with the location of the propellant grain slots. Because these grain features burn out rather quite quickly, the erosion rates at the section in line with the propellant grain slots are probably quite high initially. The maximum erosion thickness at the section in line with the propellant slots for propellant *P* was observed at the middle location (station no. 5) of the convergent part of the entrance liner, and its thickness was 11.8 mm. However, the erosion thickness at the section between the propellant slots was 3.0 mm. The difference is due to the asymmetric mass flux distributions caused by the slots. Moreover, as described in detail by Chaouat [7], for the three-dimensional nature of the SRM internal flow due to aft slots of the propellant grain, the vortices shed from grain slots create asymmetric cross-sectional flow. Because the vortical flow affects the diffusion velocity of the mass and the heat crossing the surface boundary layer on the liner materials, it causes circumferentially asymmetric erosion over the converging part of the nozzle. Propellant *P* has the larger size particles than propellant *H*, as shown in Fig. 2, and the number of particles impinging on the entrance liner surface for propellant *P* is more than that of propellant *H* because the large aluminum oxide particles move straightly due to their larger inertia. Therefore, Al_2O_3

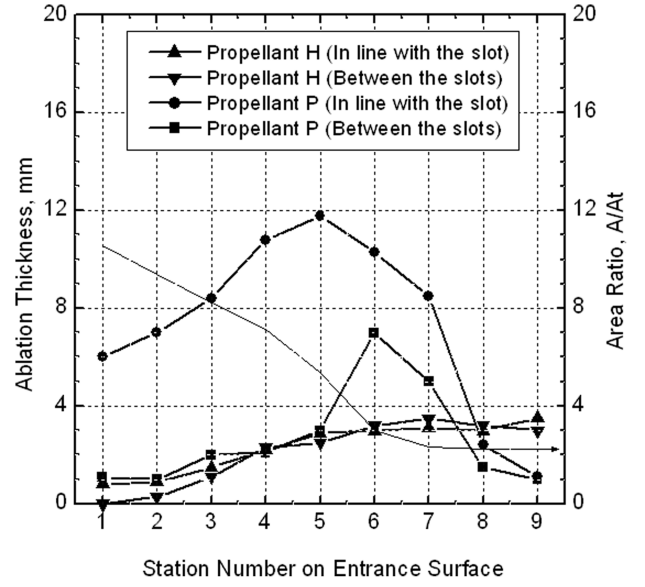

Fig. 6 Comparison of ablation thicknesses at two sections of entrance for propellants *H* and *P*.

Fig. 7 Posttest views of nozzle entrance: a) propellant *H* and b) propellant *P*.

particle sizes as well as the propellant grain asymmetries appear to have significant influence on the asymmetry erosion on the entrance liner surface.

Figure 8 shows the weight reduction of the entrance liners, as a function of motor burning time after firing tests, for a total of 14 rocket motors (6 for propellant H and 8 for propellant P). The average weight of entrance liners before the firing tests was 1600 g. The weight reductions of six entrance liners for propellant H were nearly the same, regardless of the change in motor burning time due to the difference of initial propellant temperatures ($+60$, $+20$, and -40°C), and the average weight reduction of the entrance liners was 333 g, which is 21% of the initial liner weight. However, the weight reduction of the entrance liners for propellant P increased as the burning time increased. The reduction was 478 g at 8.5 s and 624 g at 11.38 s. The number of the larger size particles causing erosion on the liner surface for propellant P is more than that for propellant H. Therefore, the burning time for propellant P has a significant effect on the weight loss, due to particle impingement erosion.

The mechanical erosion by the impingement of aluminum oxide particles is negligible on the blast tube inner surface, which is nearly parallel to the centerline of the rocket nozzle, whereas the thermochemical ablation by oxidizing species is dominant on the surface. As shown in Fig. 5, the ablation thickness of the blast tube is greater for propellant H than propellant P due to the difference of the amount of oxidizing species. The ablation thickness and char depth for propellant H were nearly the same in the upper and lower sections of the blast tube, and the ablation thickness at the middle regions (station nos. 10–14) was 2.5–3.0 mm. However, the ablation thickness for propellant P was relatively smaller than that for propellant H, and the influence of grain slots was slightly shown. The ablation thickness at the section in line with the grain slots was 1.0–1.8 mm, and the ablation thickness at the section between the slots was 0.6–1.0 mm. Therefore, the average ablation thickness of the blast tube for propellant H is about twice as deep as that for propellant P, and it must be noted that this difference in the ablation thickness is nearly consistent with the one in the oxidizing potential [B_m in Eq. (5)] for propellants H and P.

Figure 9 shows the weight reduction of blast tube liners as a function of motor burning time after firing tests for a total of 11 rocket motors (5 for propellant H and 6 for propellant P). The average weight of the blast tube liners before the firing tests was 1411 g. The average weight reductions of the blast tube liners for propellants H and P were 383 g (27% of initial weight) and 273 g (19% of initial weight), respectively. As shown in Fig. 9, the weight reductions were nearly the same, regardless of the change in motor burning time due to the difference of initial propellant temperatures. This can be explained by examining the convective heat energy in a rocket nozzle. The lower the propellant temperature before firing tests, the longer the motor burning time, but the lower the motor pressure. Therefore, the convective heat energy, regardless of the change in propellant temperature, is nearly the same because the energy is proportional to $P^{0.8} \times \tau$, where P and τ represent chamber pressure and burning time, respectively [26].

Figure 10 compares the ablation thicknesses at two sections of the throat insert for propellants H and P. Included in the figure are the area ratios for each station number along the throat insert surface. The average ablation thickness at the front position (station no. 18) of the throat insert for propellant H was 6.2 mm, and that for propellant P was 3.9 mm. This presumably comes from the difference of the ablation thickness at the blast tube liner, which is greater for propellant H than for propellant P. As shown in Figs. 5 and 10, the ablation thicknesses of the throat insert at the section in line with the grain slots were greater than those at the section between the grain slots. Moreover, the difference of ablation thickness was more prominent for propellant P, and the most difference is seen at the inclined region (station no. 20) in front of the nozzle throat by the effect of Al_2O_3 particle impingement. Because the flow velocity in the throat region is larger than that in the entrance region, there also exists a slight circumferential effect due to the propellant grain in the throat region for propellant H.

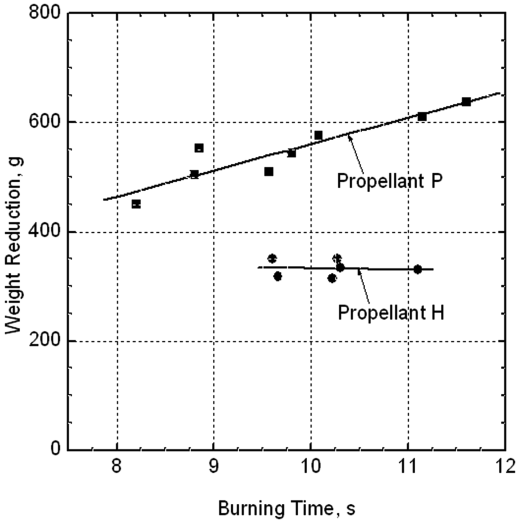

Fig. 8 Comparison of weight reduction of entrance liners for propellants *H* and *P*.

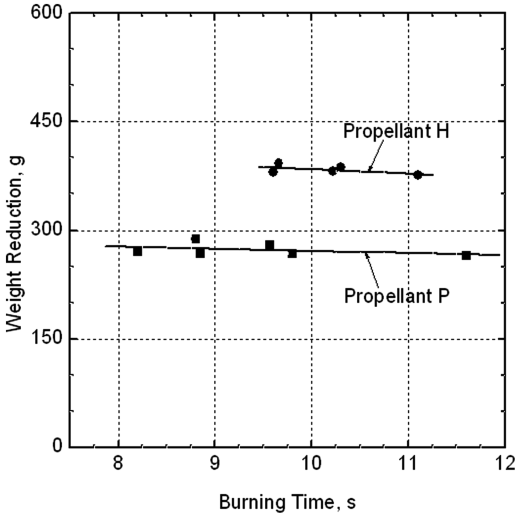

Fig. 9 Comparison of weight reduction of blast tube for propellants *H* and *P*.

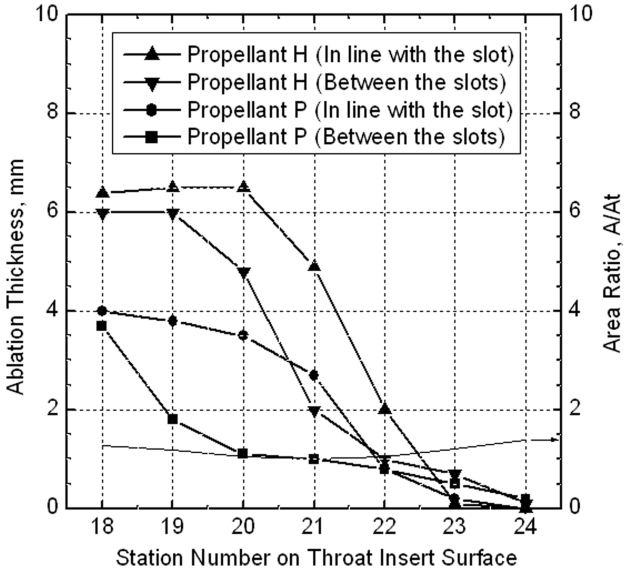

Fig. 10 Comparison of ablation thicknesses at two sections of throat insert for propellants *H* and *P*.

Figure 11 shows the ablation rate of the nozzle throat as a function of chamber pressure after firing tests for a total of 16 rocket motors (6 for propellant *H* and 10 for propellant *P*). The ablation rate increases with increasing pressure. An increase in the pressure causes an increase in the density of the gas phase. The mass transfer rate across the turbulent boundary layer is directly proportional to the density. Therefore, an increase in the pressure results in an increased supply of oxidizing species across the boundary layer to the nozzle surface. The ablation rate for propellant *H* is higher than that for propellant *P*, due to the difference of the mole fraction of oxidizing the species (H_2O and CO_2). Also, both propellants show the same linear variation of the ablation rate at the nozzle throat with the chamber pressure.

Figure 12 shows the weight reduction of throat inserts as a function of motor burning time after firing tests for a total of 12 rocket motors (5 for propellant *H* and 7 for propellant *P*). The average weight of the throat inserts before the firing tests was 400 g. The weight reductions for each propellant were nearly the same, regardless of the motor burning time. The average weight reductions of the throat inserts for propellants *H* and *P* were 74 g (19% of initial weight) and 47 g (12% of initial weight), respectively. The weight reduction for propellant *H* is greater than that for propellant *P*. The reason is considered that the thermochemical ablation by the diffusion of the oxidizing species (H_2O and CO_2) to the nozzle throat surface is more dominant than the mechanical erosion due to Al_2O_3 particles impinging on the throat insert.

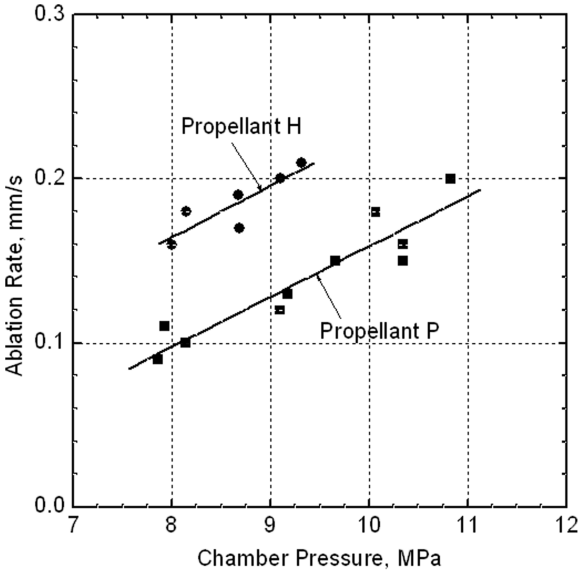

Fig. 11 Effect of chamber pressure on ablation rate at nozzle throat for propellants *H* and *P*.

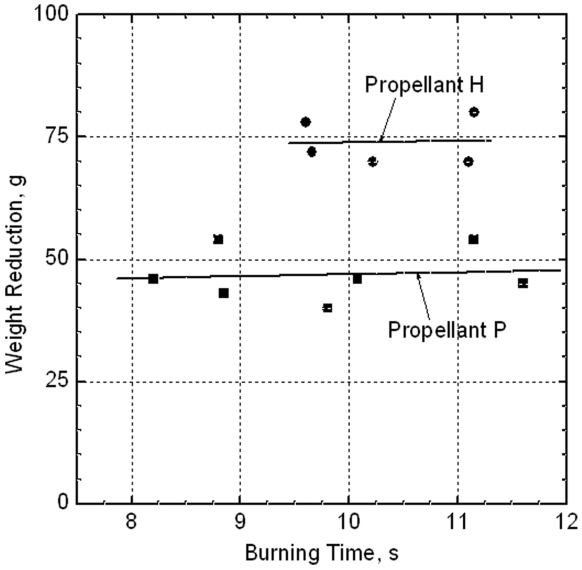

Fig. 12 Comparison of weight reduction of throat inserts for propellants *H* and *P*.

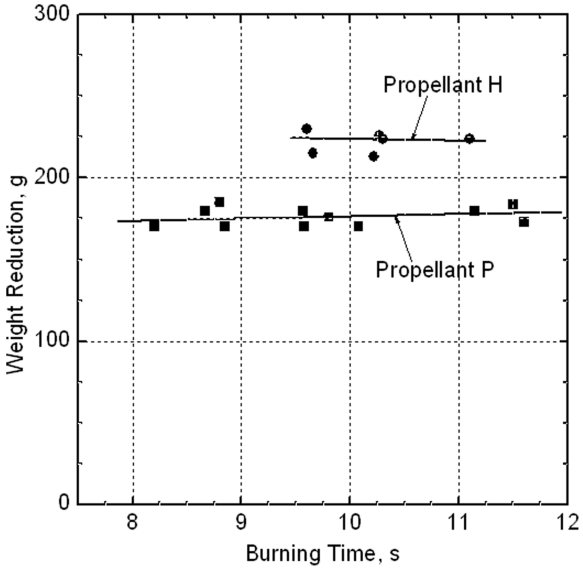

Fig. 13 Comparison of weight reduction of exit cone liners for propellants *H* and *P*.

As shown in Fig. 5, there was little ablation (erosion) at the exit cones for the two propellants. However, the char depth for propellant *H* was thicker than that for propellant *P*. The char depth for propellants *H* and *P* were 3.5–5.5 mm and 3.1–4.5 mm, respectively. Figure 13 shows the weight reduction of exit cone liners as a function of motor burning time after firing tests for a total of 17 rocket motors (6 for propellant *H* and 11 for propellant *P*). The average weight of exit cone liners before the firing tests was 1340 g. The weight reductions for each propellant were nearly the same, regardless of the motor burning time. The average weight reductions of exit cone liners for propellants *H* and *P* were 222 g (17% of initial weight) and 176 g (13% of initial weight), respectively. The char depth and weight reduction of exit cone liners for propellant *H* were greater than those for propellant *P*. The greater char depth and weight reduction for propellant *H* are related to not only the thermochemical ablation, but also to the internal behaviors of the thermodegradable material (carbon–phenolic), such as the mass loss due to pyrolysis, the associated energy absorption, the internal convection cooling effect, the thermal cracking of the gaseous phase, and so on [27,28]. On the base of the firing test data for the char depth and weight reduction of the exit cone, it is worth noting that propellant *H*, with a relatively higher mole fraction of H_2O and CO_2 in the combustion gases, may offer more favorable conditions for the density change in the exit cone liner than propellant *P*.

IV. Conclusions

The thermal characteristics of nozzle liners for a solid rocket motor with slotted tube grain containing propellant *P* or *H* have been investigated. Based on the experimental results obtained from several firing tests, the following conclusions are drawn:

1) Particle sizes of Al_2O_3 for propellant *P* were relatively larger than those for propellant *H* because propellant *P* with energetic plasticizers and bimodal oxidizers offers much more favorable conditions for increasing aluminum agglomeration than propellant *H*. However, propellant *H* has about twice as much as propellant *P* for the mole fraction of H_2O and CO_2 oxidizing species occurring to the thermochemical ablation of the nozzle liner.

2) The ablation thickness and char depth of the entrance liners for propellant *H* were almost uniform with circumferential angle, but

four higher erosion regions for propellant *P* were observed at approximately 90 deg intervals in the circumferential direction in line with the propellant grain slots. The weight reduction of the entrance liners after firing tests for propellant *P* increased as the burning time increased, due to the Al_2O_3 particles impinging on the liner surface.

3) The weight reductions of all liners (i.e., the blast tube, the throat insert, and the exit cone), except the entrance liner, after firing tests were found to be relatively greater for propellant *H* than propellant *P*, due to the thermochemical response of the liners with H_2O and CO_2 in combustion gases. Moreover, the weight reductions of each liner after firing tests were nearly the same for equal propellant, regardless of the change in motor burning time due to the difference of initial propellant temperatures.

References

[1] Douglass, H. W., Collins, J. H., Jr., Ellis, R. A., and Keller, R. B., Jr., "Solid Rocket Motor Nozzles, Space Vehicle Design Criteria (Chemical Propulsion)," NASA SP-8115, 1975.

[2] Hwang, K. Y., and Kang, Y. G., "Two-Dimensional Thermal Analysis for Carbonaceous Thermal Liner of Rocket Nozzle with Ablation and In-Depth Pyrolysis," *Journal of the Korean Society of Propulsion Engineers*, Vol. 3, No. 2, 1999, pp. 37–47.

[3] Ketner, D. M., and Hess, K. S., "Particle Impingement Erosion," AIAA Paper 79-1250, June 1979.

[4] Devenas, A., "Development of Modern Solid Propellants," *Journal of Propulsion and Power*, Vol. 19, No. 6, 2003, pp. 1108–1128.

[5] Sutton, G. P., *Rocket Propulsion Elements*, 6th ed., Wiley, New York, 1992, pp. 416–455.

[6] Shimada, T., Sekiguchi, M., and Sekino, N., "Flow Inside a Solid Rocket Motor with Relation to Nozzle Inlet Ablation," *AIAA Journal*, Vol. 45, No. 6, 2007, pp. 1324–1332. doi:10.2514/1.22952

[7] Chaouat, B., "Flow Analysis of a Solid Propellant Rocket Motor with Aft Fins," *Journal of Propulsion and Power*, Vol. 13, No. 2, 1997, pp. 194–196.

[8] Morstadt, R. A., "A 3-D CFD Analysis of the Space Shuttle RSRM with Propellant Fins @ 1s Burn-Back," AIAA Paper 2003-5105, July 2003.

[9] Yim, Y. J., "Tendency in Solid Propellant Technology for Missiles," *Journal of the Korean Society of Propulsion Engineers*, Vol. 9, No. 4, 2005, pp. 112–120.

[10] Price, E. W., "Combustion of Metalized Propellants," *Fundamentals of Solid-Propellant Combustion*, Edited by K. K. Kuo and M. Summerfield, Vol. 90, Progress in Astronautics and Aeronautics, AIAA, New York, 1984.

[11] Srinivas, V., and Chakravarthy, S. R., "Computer Model of Aluminum Agglomeration on Burning Surface of Composite Solid Propellant," *Journal of Propulsion and Power*, Vol. 23, No. 4, 2007, pp. 728–736. doi:10.2514/1.24797

[12] Sambamurthi, J. K., Price, E. W., and Sigman, R. K., "Aluminum Agglomeration in Solid-Propellant Combustion," *AIAA Journal*, Vol. 22, No. 8, 1984, pp. 1132–1138.

[13] Cohen, N. S., "Pocket Model for Aluminum Agglomeration in Composite Propellants," *AIAA Journal*, Vol. 21, No. 5, 1983, pp. 720–725.

[14] Hermsen, R. W., "Aluminum Oxide Particle Size for Solid Rocket Motor Performance Prediction," *Journal of Spacecraft and Rockets*, Vol. 18, No. 6, 1981, pp. 483–490.

[15] Johnston, W. A., Murdock, J. W., Koshigoe, S., and Than, P. T., "Slag Accumulation in the Titan Solid Rocket Motor Upgrade," *Journal of Propulsion and Power*, Vol. 11, No. 5, 1995, pp. 1012–1020.

[16] Boraas, S., "Modeling Slag Deposition in the Space Shuttle Solid Rocket Motor," *Journal of Spacecraft and Rockets*, Vol. 21, No. 1, 1984, pp. 47–54.

[17] Bui, D. T., Atwood, A. I., and Atienza Moore, T. M., "Effect of Aluminum Particle Size on Combustion Behavior of Aluminized Propellants in PCP Binder," *Proceedings of the 35th International Annual Conference of ICT*, Vol. 27, edited by M. Wolff, Fraunhofer-Inst. für Chemische Technologie, Pfinztal, Germany, 2004, pp. 27.1-27.14.

[18] Dokhan, A., Price, E. W., Seitzman, J. M., and Sigman, R. K., "Combustion Mechanisms of Bimodal and Ultra-Fine Aluminum in AP Solid Propellant," AIAA Paper 2002-4173, July 2002.

[19] Lengellé, G., Duterque, J., and Trubert, J. F., "Combustion of Solid Propellants," *RTO/VKI Special Course on Internal Aerodynamics in Solid Rocket Propulsion*, NATO Research and Technology Organization RTO-EN-023 [online database], http://www.rta.nato.int/Pubs/RDP.asp?RDP=RTO-EN-023 [cited 14 Dec. 2007].

[20] Hwang, C. J., and Chang, G. C., "Numerical Study of Gas-Particle Flow in a Solid Rocket Nozzle," *AIAA Journal*, Vol. 26, No. 6, 1988, pp. 682–689.

[21] Klager, K., "Interaction of the Efflux of Solid Propellants with Nozzle Materials," *Propellants and Explosives*, Vol. 2, No. 3, 1977, pp. 55–63. doi:10.1002/prep.19770020304.

[22] Lapp, P., and Quesada, B., "Analysis of Solid Rocket Motor Nozzle," AIAA Paper 92-3616, June 1992.

[23] Keswani, S. T., Andiroglu, E., Campbell, J. D., and Kuo, K. K., "Recession Behavior of Graphitic Nozzles in Simulated Rocket Motors," *Journal of Spacecraft and Rockets*, Vol. 22, No. 4, 1985, pp. 396–397.

[24] Borie, V., Brulard, J., and Lengellé, G., "Aerothermochemical Analysis of Carbon–Carbon Nozzle Regression in Solid-Propellant Rocket Motors," *Journal of Propulsion and Power*, Vol. 5, No. 6, 1989, pp. 665–673.

[25] Boyarintsev, V. I., and Zvyagin, Yu. V., "Turbulent Boundary Layer on Reacting Graphite Surface," *Proceedings of the 5th International Heat Transfer Conference*, Edited by N. G. Kaigi, K. K. Kyōkai, and N. K. Gakkai, Japan Society of Mechanical Engineers and Society of Chemical Engineers, Tokyo, Sept. 1974, pp. 264–268.

[26] Bartz, D. R., "Turbulent Boundary-Layer Heat Transfer from Rapidly Accelerating Flow of Rocket Combustion Gases and of Heated Air," *Advances in Heat Transfer*, Vol. 2, edited by J. P. Hartnett and T. F. Irvine, Academic, New York, 1965.

[27] Laturelle, F., Fiorot, S., and Wertheimer, T. B., "MSC.Marc-ATAS: Advanced Thermal Analysis Software for Modeling of Rocket Motors and Other Thermal Protection Systems," *MSC Aerospace Conference* [online database], http://www.mscsoftware.com/events/aero2002/partner/fullpaper.cfm?Start=41, [cited 14 Dec. 2007].

[28] Potts, R. L., "Hybrid Integral/Quasi-Steady Solution of Charring Ablation," AIAA Paper 90-1677, June 1990.

S. Son
Associate Editor